9-15-2023

Harnessing the power of metal-organic frameworks to develop microplastic fouling resistant forward osmosis membranes

Mitra Golgoli
Edith Cowan University

Javad Farahbakhsh
Edith Cowan University

Abdul H. Asif
Edith Cowan University

Mehdi Khiadani
Edith Cowan University

Amir Razmjou
Edith Cowan University

See next page for additional authors

10.1016/j.memsci.2023.121766
Golgoli, M., Farahbakhsh, J., Asif, A. H., Khiadani, M., Razmjou, A., Johns, M. L., & Zargar, M. (2023). Harnessing the power of metal-organic frameworks to develop microplastic fouling resistant forward osmosis membranes. Journal of Membrane Science, 682, article 121766. https://doi.org/10.1016/j.memsci.2023.121766

Journal of Membrane Science 682 (2023) 121766

Contents lists available at ScienceDirect

Journal of Membrane Science

journal homepage: www.elsevier.com/locate/memsci

Harnessing the power of metal-organic frameworks to develop microplastic fouling resistant forward osmosis membranes

Mitra Golgoli [a], Javad Farahbakhsh [a], Abdul Hannan Asif [a], Mehdi Khiadani [a], Amir Razmjou [a,b,c], Michael L. Johns [d], Masoumeh Zargar [a,c,*]

[a] School of Engineering, Edith Cowan University, 270 Joondalup Drive, Joondalup, Perth, WA, 6027, Australia
[b] UNESCO Centre for Membrane Science and Technology, School of Chemical Engineering, University of New South Wales, Sydney, NSW, 2052, Australia
[c] Mineral Recovery Research Center (MRRC), School of Engineering, Edith Cowan University, Joondalup, Perth, WA, 6027, Australia
[d] Fluid Science & Resources Division, Department of Chemical Engineering, The University of Western Australia, Crawley, WA, 6009, Australia

ARTICLE INFO

Keywords:
Forward osmosis
Reverse salt flux
Metal-organic frameworks
Fouling
Microplastics

ABSTRACT

With the gradual increase of microplastics (MPs) in water and wastewater streams, it is imperative to investigate their removal using tertiary treatment systems to minimize and preferably prevent their entrance into aquatic environments. Forward osmosis (FO) is a non-pressurized membrane process with potential applications in MPs removal from wastewater. However, efficient application of FO systems relies on developing high-performance FO membranes with low fouling tendency. MPs are proven as emerging foulants in membrane systems, diminishing their performance and lifetime and this highlights the need to consider MP fouling in developing sustainable membranes. The current study focuses on a novel modification of thin film composite (TFC) FO membranes by MIL-53(Fe) as a water-stable and hydrophilic metal-organic framework. Experimental results demonstrated that the optimized FO membrane (0.2 wt% MIL-53(Fe)) achieved a significantly higher water flux (90% increase) with a 23% less reverse salt flux. The modified membrane also had significantly less flux decline in fouling experiments and higher flux recovery after physical cleaning compared to the control membrane affirming its higher antifouling efficiency. MIL-53(Fe) integration in the FO substrate proved to be a practical method for developing high-performance TFC FO membranes with improved antifouling properties against MPs and organic foulants.

1. Introduction

Microplastics (MPs), plastic particles smaller than 5 mm, have become a ubiquitous problem worldwide as their presence in aquatic systems causes health risks for animals and humans owing to their potential biological toxicity at a molecular level [1,2]. MPs have been recognized as an urgent global problem by the World Health Organization (WHO), indicating the necessity to control their entrance into aquatic environments [3]. Wastewater treatment plants (WWTPs) play a significant role in increasing MP contamination in aquatic environments [4–6]; Simon et al. [7] estimated the concentration of MPs in the size ranges of 10–500 μm in the effluent of Danish WWTPs to be between 19 and 447 MP/L that leads to a discharge of around 3 tons of MPs per year from Danish WWTPs alone. Hence, advancements in wastewater treatment technologies are required to control MP entrance to waterways via the effluents of WWTPs. Forward osmosis (FO) has attracted attention from researchers to be employed as an encouraging system for treating complex wastewater streams [8–10]. FO process is a sustainable approach to removing MPs and other emerging contaminants from wastewater [11,12].

FO system uses osmotic pressure difference to drive water from the feed solution (FS) across a FO membrane to the draw solution (DS) without using hydraulic pressure [13,14]. Currently, thin film composite (TFC) membranes are the most common membranes used for the FO process. Unlike pressure-driven membrane processes, in the FO process, no pressure and temperature are exerted, that reduces capital expenditure (CAPEX) and operating expense (OPEX) making it a suitable wastewater treatment method [15]. However, the technical feasibility and practical utility of the FO process strongly rely on the performance of FO membranes (i.e., high water permeability, low reverse salt flux (RSF), and high fouling-resistant characteristics) [16–18]. RSF is defined as the permeation of draw solute from the DS into the FS that results in

* Corresponding author. School of Engineering, Edith Cowan University, 270 Joondalup Drive, Joondalup, Perth, WA, 6027, Australia.
E-mail address: m.zargar@ecu.edu.au (M. Zargar).

https://doi.org/10.1016/j.memsci.2023.121766
Received 21 February 2023; Received in revised form 19 May 2023; Accepted 20 May 2023
Available online 20 May 2023

decreasing the driving force, increasing the need, and subsequently the cost of regenerating and replenishing the DS [9,19–22]. Moreover, the salt diffusion through the porous substrates causes serious internal concentration polarization (ICP) in the substrate layer, decreasing the effective osmotic driving force and subsequently reducing water flux [15,23]. RSF is associated with the characteristics of the DS and membrane [9]. An ideal semipermeable membrane prevents the permeation of any dissolved draw solute into the FS. Fouling is another performance indicator for FO membranes. Although fouling propensity of FO membranes is lower than that of the pressure-driven membranes, it can still be detrimental to the FO performance [24–27]. Therefore, fouling mitigation of FO membranes has been a key focus of recent research in the field. Collectively, water flux, RSF, and fouling are closely interrelated in the FO process [28]. Through optimizing substrate and/or active layer properties, TFC FO membranes with high water flux, low RSF, and low fouling propensity can be developed [17].

One of the main approaches to enhance membrane performance is the incorporation of nanomaterials into the membrane structure (substrate or active layer). Numerous studies have modified the TFC FO membranes using various nanomaterials (e.g., carbon nanotubes, silica, graphene oxide, zwitterions) where the incorporation of the emerging nanomaterials into TFC FO membranes has resulted in better performance and antifouling properties of the membranes as detailed in the recent review papers [29–32]. However, incorporating additives in the active layer of TFC FO membranes may interfere with polyamide (PA) formation by preventing the polymer end functional groups from properly reacting, resulting in the formation of some defects and performance instability of the developed membranes [33,34]. Therefore, improving the performance of FO membranes by optimizing and modifying the substrate layer has been a key focus of recent studies. Substrate modification of TFC FO can enhance FO membrane performance and fouling behavior through impacting structural parameter (S) and PA layer formation without initiating defects in the selective PA layer; hence, it could be a more promising way to enhance the TFC FO membranes performance. For instance, the recent modifications of FO substrates, such as using reduced aliphatic polyketone [10] and poly [3-(N-2-methacryloylxyethyl-N, *N*-dimethyl)-ammonatopropanesulfonate] (PMAPS) [33], have proven to enhance the performance and antifouling characteristics of TFC FO membranes upon substrate modification.

Metal-organic frameworks (MOFs) are emerging porous materials consisting of inorganic metal ions bonded with organic linkers. The application of MOFs in membrane development has been an area of rapidly growing interest owing to their unique perceptible physicochemical properties such as high specific surface area, high porosity, mild synthesis conditions, and having both organic and inorganic properties [35–37]. The presence of organic linkers in the structure of MOFs improves the affinity between MOFs and organic polymers, forming non-covalent bonds between them that make them more compatible nanomaterials to be integrated with polymeric membranes compared to merely inorganic nanomaterials [36,38,39]. However, the application of MOFs in water treatment membranes is still in its infancy when compared with its application in gas separation membranes [40].

In the application of TFC FO membranes, MOFs such as ZIF-8 [41,42], UiO-66-NH_2 [43], MIL-53-NH_2(Al) [44], MIL-53(Al) [36], MOF-801 [38], MIL-101(Cr) [45], UiO-66 [46], UiO-66-$(COOH)_2$ [47] have been incorporated in the PA layer of TFC FO membranes with enhanced water permeability and antifouling resistance of the membranes. However, only a few studies investigated the impact of MOFs' presence in the substrates of TFC FO membranes. Ma et al. [48] incorporated UiO-66 in the substrate of TFC FO and reported improved water flux of the optimized modified membrane over the control membrane. Arjmandi et al. [49] applied MOF-5 to prepare TFC FO substrates and reported enhanced water flux of the modified TFC FO membranes. However, the antifouling characteristics of as-modified membranes were not investigated. Furthermore, as MPs are proven emerging foulants in wastewater affecting membrane performance and efficiency, exploring their impact on advanced membranes is required toward the sustainable development of membranes [118][5,50,51]. Previous studies have proven that even a small concentration of MPs (i.e., 1–10 ppm) could have significant impacts on the performance and fouling of the membranes [51,52], highlighting the need to conduct further research to better understand the impact of MPs on membranes and develop sustainable membranes resistant to MPs fouling. Despite the prospects of MOFs to improve the performance and antifouling resistance of FO membranes, no study has evaluated the modification of FO membranes with MOFs targeting the issue of MPs in wastewater. Hence, the potential of MOFs as a modifying agent in the FO substrates to improve membrane performance as well as antifouling characteristics while considering MPs as emerging pollutants in wastewater intrigued this study.

Incorporation of MOFs in the membrane for water application requires water-stable MOFs. Iron-based MIL-53 (MIL-53(Fe)) is a hydrophilic and water-stable MOF with relatively higher water stability compared to the other common MOFs (i.e., aluminum-based and copper-based MOFs) [53,54]. In addition, MIL-53(Fe) has shown a good interaction with polymeric membranes as an additive [39,55,56]. However, the incorporation of MIL-53(Fe) in the substrate of TFC FO membranes has not been reported in the literature. Therefore, the current study is evolved with the vision to explore the efficiency of incorporating MIL-53 (Fe), as a prospective additive, into the substrate layer of TFC FO membranes for tailoring the membranes' performance and properties for the first time. Herein, the membrane chemistry, morphology, performance, and antifouling behaviors were systematically evaluated. The synthesized MIL-53(Fe) was characterized using X-Ray diffraction (XRD), Fourier transform infrared spectroscopy (FTIR), scanning electron microscopy (SEM), and Brunauer-Emmett-Teller (BET). The developed membranes were characterized using XRD, FTIR, SEM, contact angle, and atomic force microscopy (AFM). The fouling experiments were conducted using solutions containing polyethylene (PE) MPs as the most common type of MPs in WWTP effluents [4,5], bovine serum albumin (BSA) as a model of organic foulants, and combined BSA and MPs.

2. Materials and methods

2.1. Materials

For this study, polysulfone granules (PSf Udel P-3500) were purchased from Solvay (Belgium). Terephthalic acid (Benzene-1,4-dicarboxylic acid (1,4-BDC)), analytical standard), Iron(III) chloride hexahydrate ($FeCl_3{\cdot}6H_2O$, ≥97%), N, *N*-Dimethylformamide (DMF, 99.8%), methanol (99.8%), 1-Methyl-2-pyrrolidinone (NMP, 99.5%), poly(vinylpyrrolidone) (PVP, MW: 10 kDa), *M*-phenylenediamine flakes (MPD, 99%), triethylamine (TEA, 99.5%), trimesoyl Chloride (TMC, 98%), n-Hexane (>99%), bovine serum albumin (BSA), and sodium dodecylbenzene sulfonate (SDBS, technical grade) were obtained from Sigma Aldrich (Australia) and were used as received without further purification. Sodium chloride (NaCl) was sourced from Chemsupply (Australia). PE microspheres with the size range of 740 nm–4990 nm and the density of 98 g/cc, were purchased from Cospheric (USA) and were supplied in dry white powder form.

2.2. MOF synthesis

MIL-53 (with the chemical formula of M(OH) ($O_2C–C_6H_4–CO_2$)) is prepared by trans bridging of a metal corner-sharing (i.e., Fe^{3+}, Al^{3+}, Cr^{3+}) linked by 1,4-benzene-dicarboxylate units forming a crystalline porous framework [36]. Briefly, 6.75 mM of $FeCl_3{\cdot}6H_2O$ and 4.5 mM of 1,4-BDC were dissolved in 40 mL DMF solution under vigorous stirring for 30 min at room temperature. The resultant solution was moved into a Teflon-lined stainless-steel autoclave (100 mL) and placed in an oven at

120 °C for 15 h. The autoclave was left to cool down. Then, the orange precipitates were collected using centrifugation at 9000 rpm for 15 min. Finally, the supernatant was removed, and the obtained MIL-53(Fe) was washed using DMF and heated methanol (40 °C) followed by centrifugation (9000 rpm and 15 min). The methanol washing was repeated three times and the precipitates were dried at 60 °C for 24 h in a conventional oven.

2.3. Membrane fabrication

Flat sheet PSf substrates were fabricated by the phase inversion method explained elsewhere [57]. Briefly, 16 wt% PSf granules and 2 wt % PVP were dissolved in an NMP solution. The solution was placed on a magnetic stirrer for 24 h and then kept unstirred for 10 h at room temperature for the degassing process. The solutions were cast on a non-woven PET fabric using a casting knife (Elcometer 3530) with 200 μm thickness followed by immediately immersing the in DI water for 10 min. The modified PSf substrate layers were prepared through the same approach with the addition of various MIL-53(Fe) concentrations (0.05, 0.1, 0.2, and 0.5 wt%) in the NMP solution followed by 30 min of sonication prior to the addition of PSf and PVP. Finally, the resulting membranes were washed with and stored in DI water at 4 °C to be used for the fabrication of the active layer of the TFC FO membranes. The prepared substrates in this manuscript are denoted as PSf0, PSf1, PSf2, PSf3, and PSf4 corresponding to the MIL-53(Fe) concentrations of 0, 0.05, 0.1, 0.2, and 0.5 wt% for the PSf layers, respectively.

The active layer of the TFC FO membrane was prepared by interfacial polymerization on the surface of the PSf substrate [58,59]. The fabricated PSf substrate was clamped inside a frame (made of two acrylic plates and a rubber gasket). Then, the membrane surface was soaked in an aqueous solution of MPD (2 wt%) and TEA (1 wt%) for 2 min, followed by the careful removal of the excessive solution on the substrate surface with an air knife until no water droplets were observed on the membrane surface. Subsequently, a TMC in n-hexane solution (0.15 wt %) was gently poured onto the MPD-soaked substrate for 1 min forming a PA layer. The excess solution was drained off and the membrane was air-dried for 2 min. The membrane was then placed in an oven at 60 °C for 3 min. Finally, the as-prepared membranes were washed thoroughly with 500 mL DI water at room temperature and stored in DI water at 4 °C for further use. The prepared TFC membranes in this manuscript are denoted as TFC0, TFC1, TFC2, TFC3, and TFC4 corresponding to the MIL-53(Fe) concentrations of 0, 0.05, 0.1, 0.2, and 0.5 wt% in the PSf substrate layers, respectively.

2.4. MOF characterizations

X-ray diffraction (XRD) was performed using a PANalytical Empyrean diffractometer operated at a voltage of 40 kV and a current of 40 mA with the Co-kα radiation (λ = 0.1789 nm). A PerkinElmer spectrometer was used to perform Fourier transform infrared spectroscopy (FTIR) in the range of 450–4000 cm^{-1}. Micromeritics Tristar II Plus was used to obtain the N_2 adsorption-desorption isotherms and to analyze the specific surface area and pore size distribution. The samples were degassed for 5 h in a vacuum (at 110 °C) before the BET analysis. SEM images of the coated sample (a 10 nm layer of platinum) were obtained by using field emission scanning electron microscopy (FESEM, FEI Verios 460).

2.5. Membrane characterization

The functional groups of membrane surfaces were determined by attenuated total reflectance Fourier transform infrared spectroscopy (ATR-FTIR Spectrometer, PerkinElmer). The ATR sensor was cleaned with ethanol prior to each test. XRD patterns of the membranes were obtained at a rate of 0.01°/s using a PANalytical EMPYREAN diffractometer. The surface and cross-sectional morphology and topography of the membranes) were examined using the FESEM (FEI Verios 460). Cross-section samples were prepared by peeling the membranes from the PET supports followed by submerging the peeled samples in a container of liquid nitrogen using a tweezer for a few seconds. The frozen membranes were then taken out and immediately fractured. All membrane samples were then dried for a few hours, mounted on aluminum stubs, and sputter coated with platinum (10 nm) using Polaron SC7640 sputter coater. SEM images were obtained at a voltage of 3–5 kV and a working distance of 5–7 mm. Energy-dispersive X-ray (EDX) spectroscope was used to acquire the elemental composition of the membranes with a voltage of 20 kV, and a working distance of 5.5 mm. Atomic force microscopy (AFM, Nanosurf model C3000) was used to explore the roughness and 3D morphology of the membrane surfaces with a scanning area of 5 μm × 5 μm. Membrane samples were air-dried in a protected sample box (to avoid any contamination) for a few hours before analysis. Three replicates were done where the average results were reported. The contact angles of membranes were measured by an Attention Theta Optical tensiometer. At least five different points of each sample were measured, and the results were averaged. The porosity (ε) of the PSf substrates was calculated using:

$$\varepsilon = \frac{(W_w - W_d)/\rho_w}{(W_w - W_d)/\rho_w + W_d/\rho_p} * 100 \quad \text{(Equation 1)}$$

where W_w is the weight of the wet membrane with no excess water on the surfaces, W_d is the dry membrane after overnight drying at 60 °C, ρ_w is the density of water and ρ_p is the density of the polymer [60]. Three samples were measured, and the average results were reported.

2.6. FO performance evaluation

A laboratory-scale crossflow FO filtration system was used to conduct the performance analysis and fouling tests. The FO system included a membrane cell (CF016, Sterlitech), two gear pumps (Masterflex, Sterlitech) for the circulation of FS and DS, two flowmeters (Site read panel mount flowmeter, Sterlitech) for controlling the flow rates (at 0.5 L/min on both sides), and two pressure gauges to observe and control the zero hydraulic pressures on both sides. The mass change of DS (2 M NaCl with an initial volume of 2 L) was recorded using a balance (Ohaus) connected to a computer equipped with recording software. A schematic of the FO system used in this work is presented in Fig. S1. The RSF was measured by placing a conductivity meter (WTW multi-3430, Xylem Analytics) in the FS. Membrane water flux (liters per square meter hour (LMH)) was calculated using:

$$J_w = \frac{V_{d,t} - V_{d,0}}{A.t} \quad \text{(Equation 2)}$$

where J_w is the water flux, V_d is the volume of the DS, A is the surface of the membrane and t is the measurement time.

The RSF (g/m^2h) was calculated using:

$$J_s = \frac{C_t V_{f,t} - C_0 V_{f,0}}{A.t} \quad \text{(Equation 3)}$$

where J_s is the RSF, V_f is the volume and C is the salt concentration of the FS. The specific salt flux was determined as the ratio of RSF and water flux $\left(\frac{J_s}{J_w}\right)$.

To determine the transport and structural parameters of the membranes, the method developed by Tiraferri et al. [61] was followed. The method involved conducting a FO experiment in four stages using different concentrations of DS in each stage (i.e., 0.5, 1, 1.5 and 2 M NaCl). The water flux and RSF were measured in each step and these values were then used to fit the corresponding FO transport equations proposed in the method which gives the water permeability coefficient (A), the solute permeability coefficient (B), and the structural parameter (S) of the fabricated membranes.

2.7. Fouling analysis

Three different solutions containing foulants (i.e., BSA, MPs, and combined BSA and MPs) were prepared to perform fouling experiments. Synthetic wastewater of 30 mM NaCl and 1 mM $CaCl_2$ was used as the background solution that represents the similar ionic strength and ratio of Na/Ca in secondary wastewater effluents of WWTPs [62]. Humic substances and proteins were proven to cause irreversible fouling in FO systems treating secondary wastewater [63]. Here, BSA was selected as the model organic foulant to represent proteins in this study. The BSA solution was prepared by dissolving 100 ppm BSA in the background solution. This concentration was selected as the concentration of organic foulants in real wastewater are normally between 40 and 140 ppm [64]. The FS containing MPs was prepared by 10 ppm of PE MPs (740 nm–4990 nm) and 0.1% SDBS surfactant in the background solution. PE MPs were used as a model of MP foulants as they are the most abundant type of MPs in the effluent of WWTPs [4,5]. SEM image (Fig. S2), FTIR spectra (Fig. S3) and the zeta potential measurement data of the MPs are presented in the Supplementary Information file. The 10 ppm concentration of MPs was used in this work as per the data reported in a recent study exploring MPs in different stages of three WWTPs [65]. The calculation of MPs' concentration based on the adapted date from the reference study is presented in the Supplementary Information file. The SDBS surfactant was used to form a more uniform suspension of MPs simulating their presence in real wastewater [66]. The FSs containing BSA, and MPs were used to study the combined fouling of organic foulants and MPs. Each fouling test was run for 22 h at a crossflow velocity of 8 cm/s. The normalized flux J^* was calculated from:

$$J^* = \frac{J}{J_0} \quad \text{(Equation 4)}$$

where J_0 was the initial permeate flux.

The physical cleaning of membranes was performed using DI water on both sides of the FO system with a crossflow velocity of 16 cm/s for 30 min [63]. Then, refreshed DS and DI water were used to determine the water flux under the same initial conditions (i.e., 2 L of 2 M NaCl as the DS, 4 L of DI water as the FS, and a crossflow velocity of 8 cm/s on both sides). The flux recovery rate was measured using:

$$\textit{Flux Recovery Rate}\ (\%) = \frac{J_c}{J_0} \times 100 \quad \text{(Equation 5)}$$

where J_c and J_0 are the water flux after the physical cleaning (LMH) and the initial water flux of the membrane (LMH), respectively.

3. Results and discussion

3.1. MOF characterization

The X-Ray diffraction (XRD) patterns were collected to confirm the crystallinity of the synthesized MOFs. Fig. 1A depicts the sharp and clear X-ray diffraction pattern (10.8, 14.5, 21.9, highlighted peaks) of the as-synthesized MIL-53(Fe) confirming the formation of a crystalline MOF structure consistent with the literature [39,54]. FTIR spectrum of the MIL-53(Fe) is presented in Fig. 1B. The respective peaks at 749 and 547 cm^{-1} are related to the C–H band stretching of the benzene ring structure of terephthalic acid, and Fe–O band vibrations, respectively [54]. One absorption band at 1595 cm^{-1}, and two sharp vibrational modes at 1507, and 1388 cm^{-1} are ascribed to the typical C═O, and C–O band stretching, respectively confirming the presence of the BDC organic linker in the MOF structure [67]. Furthermore, the wide band vibration at 3390 cm^{-1} is assigned to the typical O–H stretching, ascribing to the adsorbed water molecules on the MOF surface [39]. Specific surface area (SSA) and porosity are critical factors in the application of porous materials in different fields. Therefore, the textural properties and porosity of the as-synthesized MIL-53(Fe) were investigated through N_2 adsorption-desorption analysis. The MIL-53(Fe) particles reflected a specific surface area of 603.75 m^2/g, and an average pore size of 2.26 nm. Fig. 1D presents the SEM image of the MIL-53(Fe) that depicts a polygonal structure with a smooth surface and cornered edges. The particles had a size range of 500–2500 nm as per the dynamic light

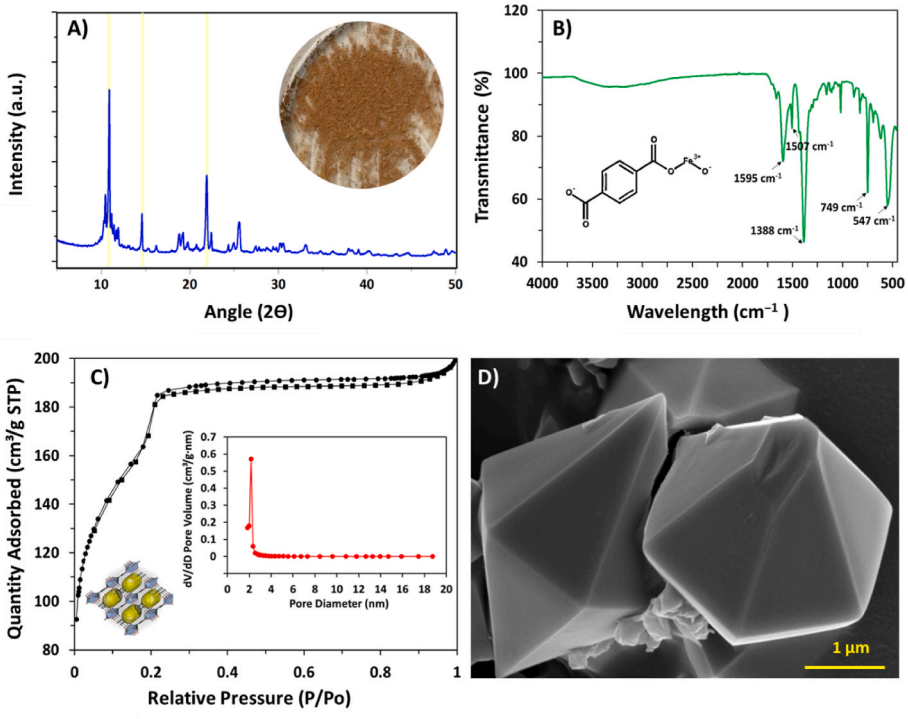

Fig. 1. (A) XRD pattern, (B) FTIR spectra, (C) N_2 adsorption-desorption isotherms and pore-size distributions, and (D) SEM image of the as-prepared MIL-53(Fe) at a magnification of 35 kx.

scattering (DLS) data reported in Fig. S4.

3.2. Membrane characterization

3.2.1. Substrate characterization

Fig. 2A shows XRD patterns of the control and modified PSf substrates. The three broad peaks in the membrane patterns are related to the ordered entanglement regions of polysulfone chains [68]. The appearance of the characteristic peak (9.9°) of MIL-53(Fe) in the modified substrates (PSf3 and PSf4) confirmed the successful incorporation of MIL-53 in the substrate matrix [69,70], however, the peak was indiscernible in PSf1 and PSf2 substrate owing to the low content of MIL-53(Fe) (i.e., 0.05% and 0.1%) in the casting solution. The incorporation of MIL-53(Fe) in PSf substrates is due to the hydrogen bonding and π-π interactions. Since MIL-53(Fe) consists of hydrogen bond acceptor sites (-OH), there is a possibility of hydrogen bond formation between the MIL-53(Fe) and PSf. Moreover, there are π-π interactions between aromatic groups of PSf and MIL-53(Fe) as illustrated in Fig. 2C [71,72]. The FTIR analysis of the substrates is presented in Fig. 2B. The FTIR spectra of all substrates showed the characteristic bands of polysulfone (PSf): i.e., 1095 cm^{-1} (skeletal aliphatic C–C/aromatic hydrogen bending/rocking), 1243 cm^{-1} (C–O–C stretching, aromatic ether stretching), 1489 cm^{-1} (C–C bond stretching), and 1583 cm^{-1} (S═O stretching) [73–77]. The appearance of new peaks at 1507 cm^{-1} and 1595 cm^{-1} (asymmetric carbonyl stretch) in the modified substrates are related to the BDC carboxylate groups of the MIL-53(Fe) (Dashed orange lines in Fig. 2B) [55]. Moreover, the new peaks observed at the wavelengths below 1300 cm^{-1} (i.e., 1287, 1150, 841, 689, and 630 cm^{-1}) can be related to the vibrations of the BDC ligand (Dashed blue lines in Fig. 2B) [67].

The surface and cross-section morphologies of the control and modified substrates were characterized by SEM (Fig. 3). The top surface of the modified substrates (Fig. 3A) confirmed the integration of MIL-53 (Fe) in PSf membranes. The cross-section images of the substrates (Fig. 3B) confirmed that all substrates had a typical asymmetric porous structure with a porous top layer and a finger-like pore structure across the membranes. It is evident that the modified substrates have several microcellular-like structures (Fig. S6) due to the rapid solvent/non-solvent exchange during the phase inversion because of the hydrophilic nature of MIL-53(Fe) particles [78]. Furthermore, the MIL-53(Fe) particles observed on the surface of the modified membranes (Fig. 3) were smaller compared to those incorporated in the cross-section of the membranes as evidenced by the cross-sectional SEM images shown in Fig. S7. This phenomenon can be attributed to the fact that the larger particles, being heavier, tend to precipitate through the support material during the phase inversion process. As a result, the larger MOF particles end up being embedded within the membrane structure, thereby leading to the observed difference in the size distribution of MOFs on the surface and within the support layer. This finding aligns with a previous study [79] investigating the incorporation of metal oxides as hydrophilic additives in polyethersulfone (PES) membranes, which also observed distinct distribution patterns of particles with different weights along the membrane structure. That was attributed to the tendency of heavier particles to precipitate towards the polyester support. The AFM images and roughness data of the PSf substrates are presented in Fig. 3C and D, respectively. The MIL-53(Fe) incorporation increased the surface roughness of the modified membranes (from 5.25 nm for PSf0 to 21.86 nm for PSf4) due to the exposure of some particles to the surface that increased by the increased concentration of the particles [80]. The porosity data are presented in Fig. 3E. The porosity of the modified substrates increased resulting from the integration of the hydrophilic MIL-53(Fe) in the polymer solution as hydrophilic additives can enhance the exchange rate between NMP (solvent) and water (non-solvent) during the phase inversion and increase the porosity of the developed membranes [81–85]. However, at the highest content of MIL-53(Fe) (PSf4, 0.5%), the porosity decreased compared to the PSf3 (0.2%) which can be correlated to the higher viscosity of the casting solution at higher additive concentrations. That causes more severe kinetic hindrance during phase inversion and results in lower porosity of membranes containing more additives [86]. That can be also attributed to the aggregation of particles at higher concentrations creating more mass transfer resistance resulting in a slower exchange rate between solvent and non-solvent during polymeric membrane formation as reported in the literature [87]. The hydrophilicity of the membranes was determined by measuring the water contact angle where data are reported in Fig. 3F. The contact angle decreases (from 64.74° for PSf0 to 50.27° for PSf4 ($P < 0.05$)) gradually with the increase of MIL-53(Fe) loading in the PSf layer due to the hydrophilic groups of MIL-53(Fe) (i.e., O–H, Fe–O, O–C═O groups) that is in agreement with the results reported in other studies integrating MOFs in polymeric membranes [54,69,88]. In addition, the contact angle is influenced by membrane porosity where can be defined by Washburn equation that is presented in the Supplementary

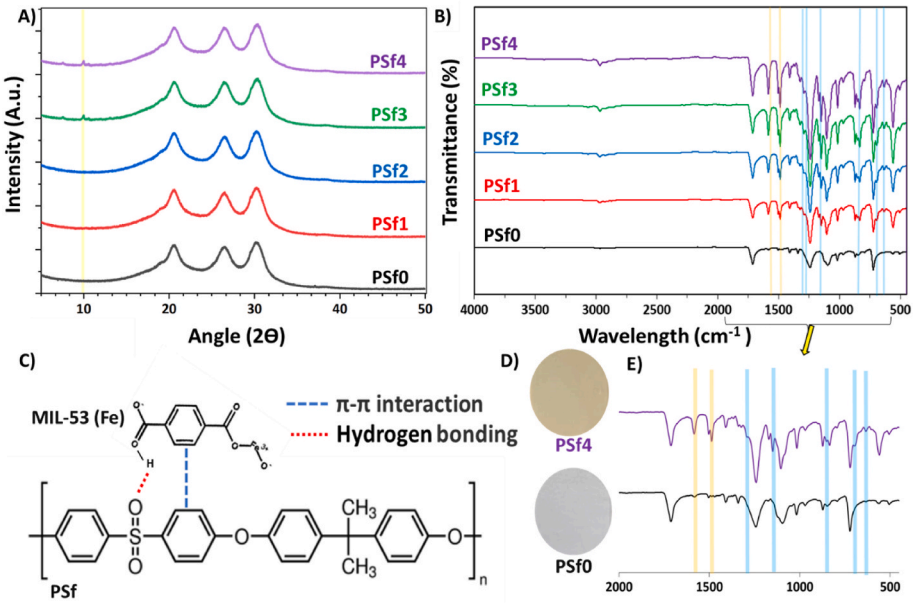

Fig. 2. (A) XRD patterns and (B) FTIR spectra of control PSf and modified PSf substrates integrated with MIL-53(Fe), (C) Schematic illustration of the interaction between PSf and MIL-53(Fe), (D) Optical images of PSf0 and PSf4, and (E) Zoomed-in view of FTIR spectra over 500- 2000 cm^{-1}. (For the color indications, please refer to the online version of the manuscript). (For interpretation of the references to color in this figure legend, the reader is referred to the Web version of this article.)

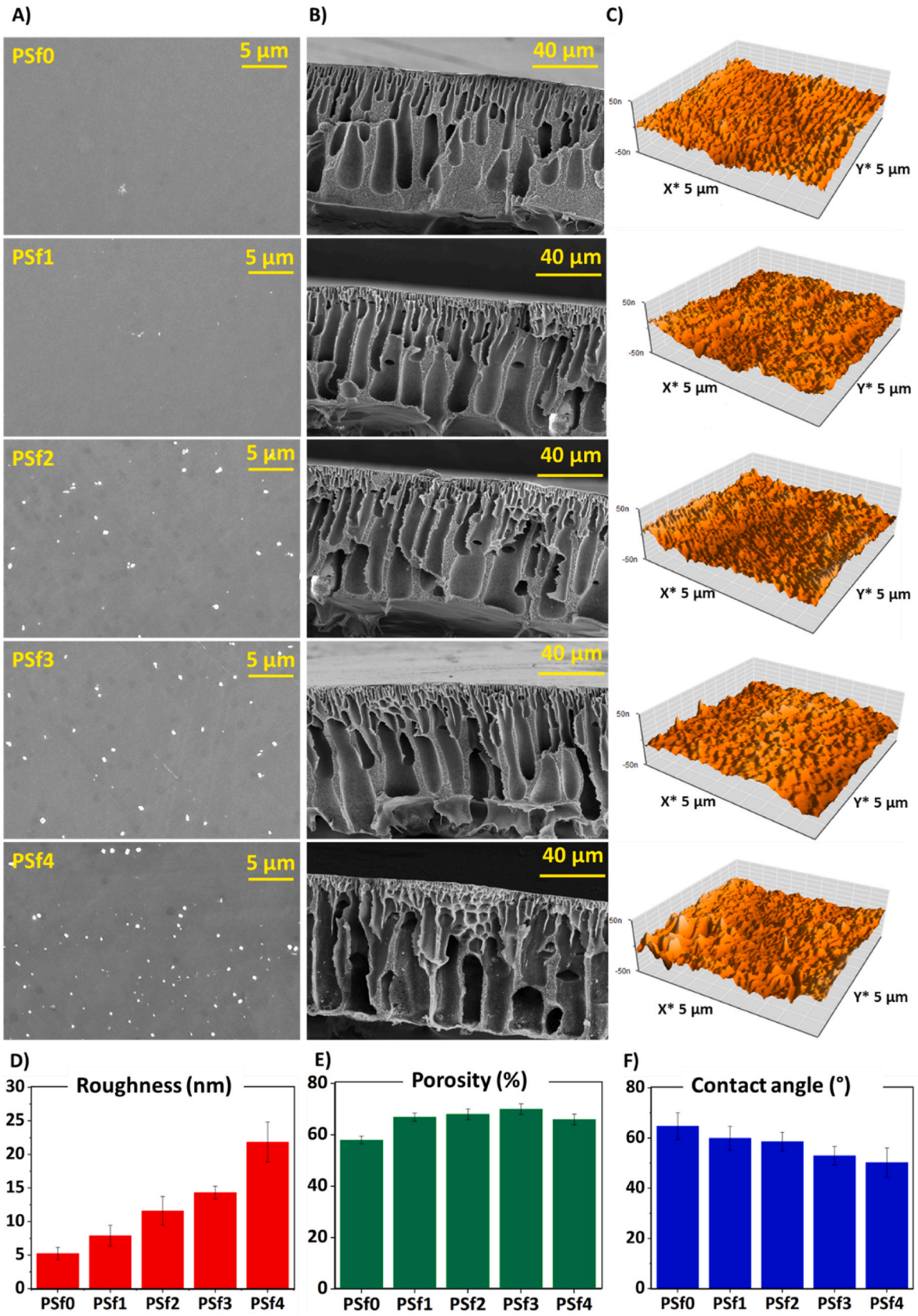

Fig. 3. (A) SEM images of top surfaces at a magnification of 6.5 kx (B) SEM images of cross-sections at a magnification of 1.2 kx (C) AFM images at a scan area of 5 µm by 5 µm (D) Roughness data, (E) Contact angle data, and (F) Porosity data of the control (PSf0) and modified PSf substrates (PSf1, PSf2, PSf3, and PSf4) with various loading of MIL-53(Fe) (0.05, 0.1, 0.2, 0.5 wt%). Standard deviations are the average of at least three replicates for roughness, seven replicates for contact angle, and three replicates for porosity.

Information file [89]. Generally, the higher porosity of the membrane results in the lower contact angle [90]. That is also the case for modified substrates (PSf1, PSf2, and PSf3) in this work, while for the PSf4 with a lower porosity compared to PSf3, the contact angle is lower. This can be attributed to the presence of more hydrophilic functional groups of MIL-53(Fe) that can significantly impact the contact angle and result in a lower contact angle despite the lower porosity of the membrane. The EDX elemental mapping of the top surface and the cross-section of the PSf4 substrate as a representative for the modified substrates is presented in Fig. S8. The EDX data confirm the presence of Fe element (hence MIL-53(Fe)) across the modified membrane.

3.2.2. TFC characterization

Fig. 4A and B presents the surface SEM images of the fabricated PA layer on the as-prepared substrates. All the TFC FO membranes showed typical ridge-and-valley surface topographies that affirmed the successful formation of the PA layer on the PSf and PSf/MIL-53(Fe) substrates by interfacial polymerization. SEM images of the TFC membranes illustrated that the PA layer on the modified substrates has a more nodular structure compared to the PA layer on the control substrate (Fig. 4B) where yellow arrows indicate the leaf-like and red arrows indicate nodular structures in the SEM images. That is related to the change of PA morphology owing to the change of the reaction rate during the interfacial polymerization. The higher porosity and hydrophilicity of the modified substrates increase the reaction rate of MPD/TEA with TMC which resulted in a more nodular structure [91]. The AFM images and surface roughness data of the TFC membranes are presented in Figs.. 4C and 4D, respectively. The surface roughness of the TFC membranes was reduced by increasing the MIL-53(Fe) loading in the substrates. These changes can be related to the morphology change of the PA layer having more nodular structure (as confirmed by SEM images) resulting in the formation of a smoother PA layer [81,92,93]. The average roughness (*Ra*) decreased from 31.21 nm for TFC0 to 19.06 nm for TFC3 while the roughness increased from 19.06 nm for TFC3 to 25.08 nm for TFC4. The change in the roughness trend is related to the fact that the substrate of TFC4 (PSf4) had lower porosity compared to that of the TFC3 (PSf3) as confirmed by the substrate characterizations (Section 3.2.1).

The surface hydrophilicity of the TFC membranes is presented in Fig. 4E. The TFC membranes made by the modified substrates showed higher hydrophilicity as compared to the control TFC membrane due to the presence of hydrophilic groups of MIL-53(Fe) on the modified substrates. This is related to the fact that a hydrophilic support layer facilitates the formation of a smoother PA layer with higher ability to swell and absorb water on its surface [94]. Therefore, the presence of hydrophilic groups of MIL-53 (Fe) on the substrate leads to the formation of a more hydrophilic PA layer. Yang et al. coated tannic acid (TA)-Fe nanoscaffold onto a PSf substrate and reported higher hydrophilicity of the formed PA layer on the coated substrate due to the presence of hydrophilic groups on the substrate [95]. Likewise, Pendergast et al. [96] reported higher hydrophilicity of TFC membranes upon integration of zeolite in the substrate. In addition, surface roughness can affect the contact angle of a liquid on a solid surface, according to the Wenzel and Cassie models. The Wenzel model applies to homogeneous surfaces, while the Cassie model considers heterogeneous surfaces composed of solid and air pockets. In the Cassie model, increasing solid roughness can lead to a higher contact angle due to the formation of air pockets within the peaks of surface features, which is consistent with the results of this study [39,97–99].

3.3. FO performance evaluation

The presence of MIL-53(Fe) in the substrates significantly impacts the performance of the resultant TFC membranes. Fig. 5 indicates the water flux, RSF, and the specific salt flux (the ratio of RSF per water flux) of the TFC FO membranes with substrates loaded with various concentrations of MIL-53(Fe). All modified membranes had higher water flux compared to the control membrane with a significant statistical difference ($p < 0.05$). The flux improvement of the modified membranes can be attributed to the modified substrate and thereby, the PA layer structure. The incorporation of MIL-53(Fe) increased the porosity and hydrophilicity of the substrates as confirmed by the data reported in Fig. 3E and F; which have been reported as effective methods in mitigating ICP in TFC FO membranes in the literature [100–102]. This increase in hydrophilicity and porosity allows for more effective transport of water and solute molecules in the substrate, reducing air entrapment in the membrane pores and resulting in a smaller structural parameter (S) of the substrate leading to lower ICP and higher water flux [86]. The decrease of the structural parameter (S) of the modified membranes was confirmed by the experimental results presented in Table 1. Similarly, research studies modifying the substrates of the FO membranes by the incorporation of other additives such as TiO_2 [103], halloysite nanotubes [104], poly(2-dimethylaminoethyl methacrylate) [85] and silicene nanosheets [87] reported the enhanced water flux of FO membranes upon nanomaterials integration in the FO substrate layers. In addition, the improved hydrophilicity of the TFC membranes is also a critical factor in increasing the diffusion rate of water molecules through the modified membranes increasing the water flux [105]. Among the developed TFC membranes, the optimal water flux was achieved for the TFC3 (0.2 wt% of MIL-53(Fe) incorporated into the substrate), with the water flux increasing from 6.0 LMH for the control membrane to 11.4 LMH for the TFC3. At the concentration of 0.5 wt% MIL-53(Fe) (TFC4), water flux decreased owing to the lower porosity of the substrate (PSf4) as explained and confirmed in the substrate characterization (Section 3.2.1). Hence, in this study, 0.2 wt% was identified as the optimum concentration of MIL-53(Fe) as an additive in the PSf substrate of FO membranes.

The presence of MIL-53(Fe) in the substrates caused a statistically significant decrease ($P < 0.05$) in the RSF of the modified membranes compared to the control membrane (from 6.3 g/m^2h for the control membrane to 5.08 g/m^2h for the TFC3 membrane). This can be attributed to the change of PA layer formation upon the integration of MIL-53 (Fe) in the substrates. The presence of hydrophilic functional groups on the substrate has been reported to promote the formation of a more uniform and defect-free/less defective PA layer due to the more uniform distribution of the amine aqueous solution on more hydrophilic substrates [106,107]. That can be the reason why in this study, the presence of MIL-53 (Fe) with hydrophilic functional groups has resulted in the reduction of RSF for the modified TFC FO membranes compared to the control one. In a recent study, She et al. [107], modified the substrate of nanofiltration (NF) membranes that resulted in higher hydrophilicity of the substrate. The improved hydrophilicity of the substrate favored the formation of a uniform defect-free PA layer that led to a better salt rejection of the modified membranes. However, it is worth noting that in the previous studies, a lower RSF was observed upon the integration of MOFs in the PA layer of TFC FO membranes that was attributed to the presence of MOFs with small pore size that could create tight pathways decreasing the diffusion of ions through the membrane [41]. For instance, Bayrami et al. incorporated MIL-53 (Al) in the PA layer of TFC FO membranes and also reported a reduction of the RSF owing to the small pore size of the incorporated MOFs [44]. Similarly, Samsami et al. reported lower RSF upon integration of MIL-53 (Al) in the PA layer of TFC FO membranes as the presence of MIL-53 (Al) makes tortuous and tight channels that reduce the diffusion path of ions resulting in lower RSF [36]. However, in this study, the reason behind this phenomenon is different as the MOFs have been integrated in the substrate. Additionally, the pore size of the integrated MIL-53 (Fe) (i.e., 2.25 nm) in this work is larger than the hydrated size of Na^+ and Cl^- ions, and hence it does not hinder their transport in the substrate. Moreover, the lower specific reverse salt flux (J_s/J_w) of the modified membranes indicates a higher FO selectivity [108]. Table 1 presents the transport parameters of the membranes which are water permeability coefficient (A), solute

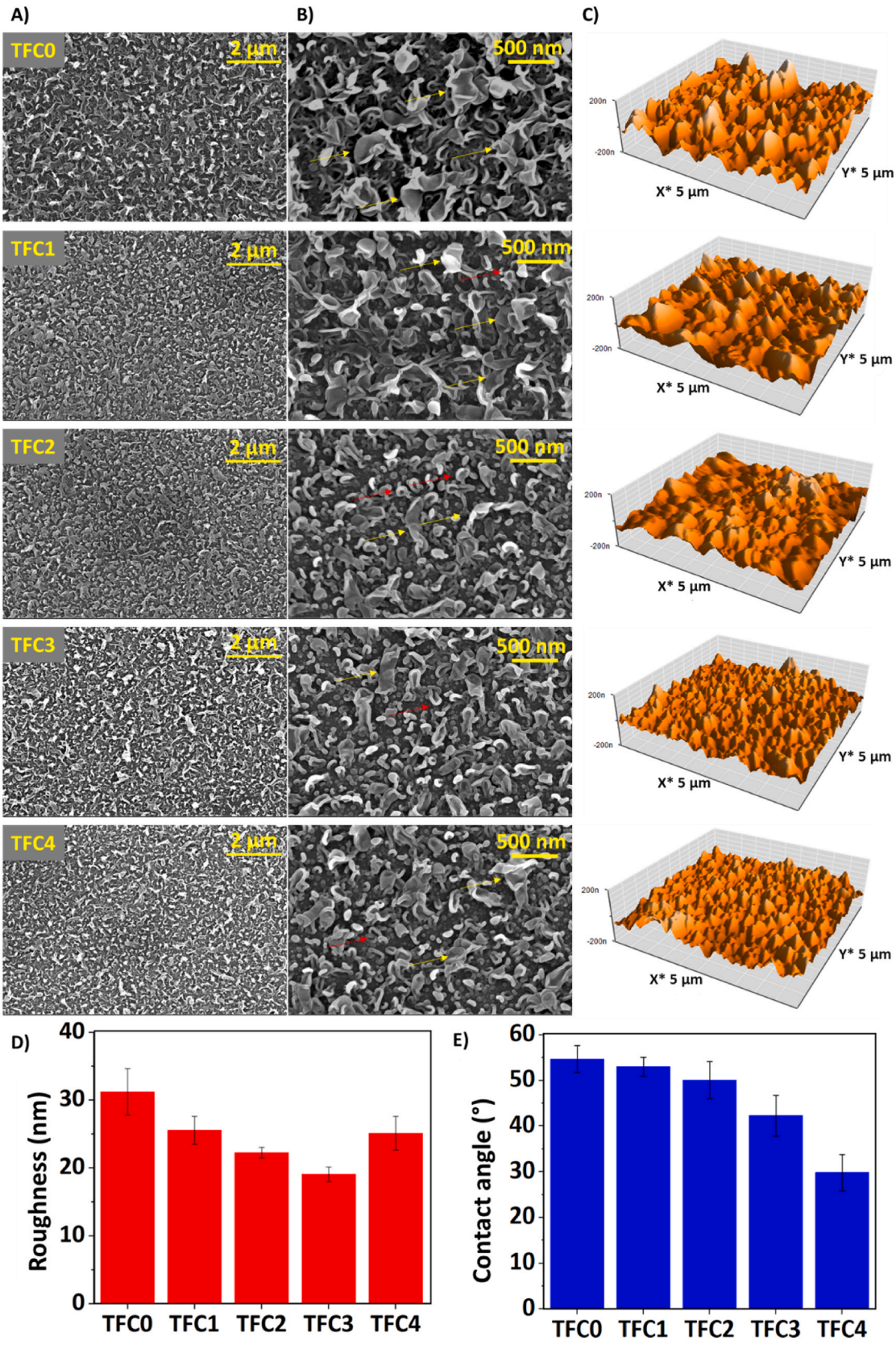

Fig. 4. (A) SEM surface images at a magnification of 20 kx, (B) Zoomed-in SEM surface images at a magnification of 65 kx, yellow arrows indicate the leaf-like and red arrows indicate nodular structures (C) AFM 3D images at a scan area of 5 µm by 5 µm, (D) Roughness data and (E) Contact angle data of fabricated TFC membranes (TFC0, TFC1, TFC2, TFC3, and TFC4) on control and modified PSf substrates by various loading of MIL-53(Fe) (0.05,0.1, 0.2, 0.5 wt%). Standard deviations are the average of three replicates for roughness and five replicates for contact angle measurements. (For the color indications, please refer to the online version of the manuscript). (For interpretation of the references to color in this figure legend, the reader is referred to the Web version of this article.)

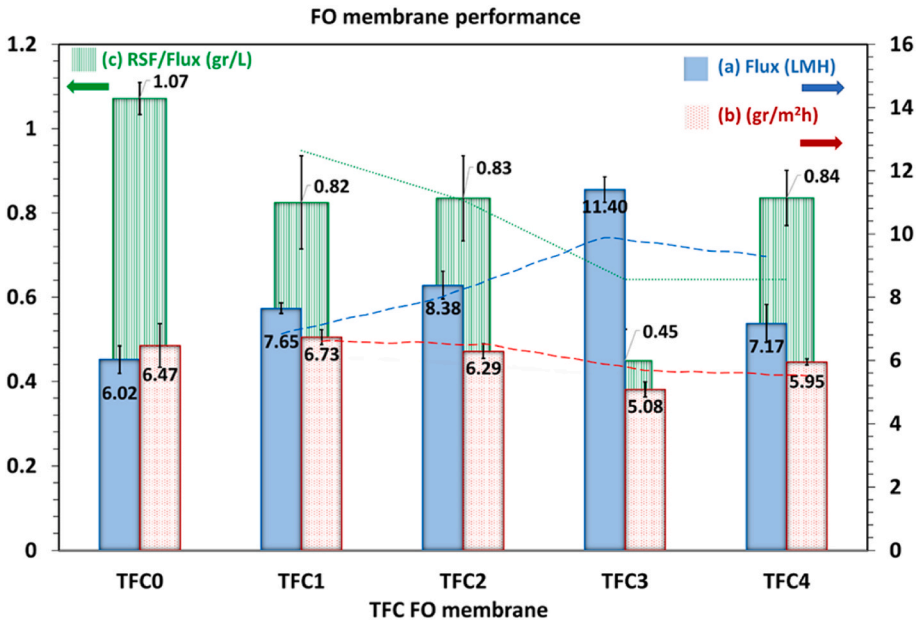

Fig. 5. Performance evaluation of prepared TFC membranes (TFC0, TFC1, TFC2, TFC3, and TFC4) on control and modified PSf substrates by various loading of MIL-53(Fe) (0.05, 0.1, 0.2, 0.5 wt%) (a) Water flux, (b) RSF, and (c) RSF/Flux. Error bars represent standard deviation from triplicate experiments. Dashed lines indicate the trendline of each parameter. Experimental conditions: DI water as the FS and 2 M NaCl as the DS; with a crossflow velocity of 8 cm/s on both sides. (For the color indications, please refer to the online version of the manuscript). (For interpretation of the references to color in this figure legend, the reader is referred to the Web version of this article.)

Table 1
The transport parameters of TFC membranes (TFC0, TFC1, TFC2, TFC3, and TFC4) on control and modified PSf substrates by various loading concentrations of MIL-53(Fe) (0.05, 0.1, 0.2, 0.5 wt%).

Membrane	A (L m^{-2} h^{-1} bar^{-1})	B (L m^{-2} h^{-1})	B/A (bar)	S (μm)
TFC0	0.297	0.271	0.91	1490
TFC1	0.359	0.269	0.75	1130
TFC2	0.453	0.283	0.62	1110
TFC3	0.615	0.228	0.37	822
TFC4	0.405	0.283	0.70	1350

permeability coefficient (B) and structural parameter (S). The results showed that the control sample (TFC0) had a lower water permeability coefficient (A) and a higher solute permeability coefficient (B) compared to the modified membranes which are consistent with the water flux and RSF trends of membranes (Fig. 5). In summary, the improved water flux, decreased RSF and the low specific reverse salt flux of the modified membranes suggest that the incorporation of MIL-53(Fe) in FO substrates is an effective approach to improve the performance of FO membranes.

3.4. Fouling analysis

Fouling experiments were conducted to evaluate the antifouling

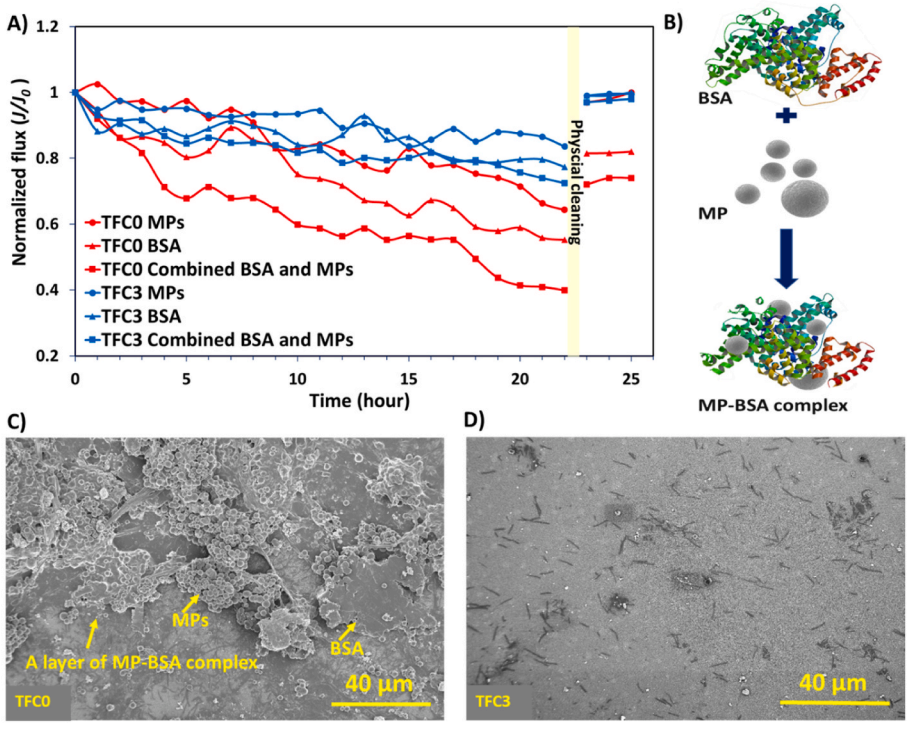

Fig. 6. (A) Normalized flux trend for TFC0 (the control membrane) and TFC3 (the optimized modified membrane with 0.2 wt% loading of MIL-53(Fe)) using three different FS containing BSA, MPs, combined BSA and MPs, Experimental conditions: 2 M NaCl as the DS; with a crossflow velocity of 8 cm/s on both sides; Fouling experiments were repeated twice and the normalized flux data were averaged and reported here. (B) Schematic illustration of MP-BSA complex formation owing to electrostatic forces. SEM images of (C) TFC0 and (D) TFC3 at magnifications of 1 kx after fouling experiments using combined BSA and MPs as FS for 22 h followed by a physical cleaning; yellow arrows indicate foulants (i.e., MP, BSA and MP-BSA complex) on the surface of TFC0; Physical cleaning condition: using DI water with a crossflow velocity of 16 cm/s on both sides. (For the color indications, please refer to the online version of the manuscript). (For interpretation of the references to color in this figure legend, the reader is referred to the Web version of this article.)

performance of the TFC0 (TFC membrane fabricated on control PSf) and TFC3 (TFC membrane fabricated on the PSf substrate with 0.2 wt% loading of MIL-53(Fe)). The normalized water flux J/J_0 of both membranes over time using different solutions containing foulants (i.e., BSA, MPs, and combined BSA and MPs) is illustrated in Fig. 6A. Initial water flux data for each group of foulants (i.e., MPs, BSA and combined BSA and MPs) are presented in Table S2. TFC0 and TFC3 membranes demonstrated flux decline of 36% and 16% against MPs, 45% and 24% against BSA, and 60% and 29% against combined BSA and MPs, respectively. Therefore, TFC3 showed lower flux decline against all foulants compared to TFC0 thus indicating the lower fouling propensity of TFC3. The better antifouling characteristic of the modified membrane can be attributed to the lower surface roughness and the higher hydrophilicity of the PA layer. The intrinsic ridge-and-valley structure of the PA layer strongly impacts the fouling propensity of the TFC membranes as the higher roughness of the PA layer (more leaf-like features on the surface) provides a larger surface for the attachment of foulants. Further, the higher roughness facilitates foulant deposition on the valley features of the rough PA surfaces [93,109]. Furthermore, the surface hydrophilicity of the PA layer also impacts the antifouling property since, in the case of the membrane with higher surface hydrophilicity, the surface gets wet quickly owing to its higher affinity toward water molecules [110]; this tendency results in adsorbing water on the surfaces and subsequently decreasing the possibility of absorbing foulants (majority of them being hydrophobic), and thereby, improving the antifouling property of the membrane. The other determining factor in the fouling of FO membranes is the RSF that causes ICP in the substrate resulting in a higher fouling rate [15,23]. Moreover, RSF aggregates the fouling due to the diffusion of salt ions to the FS, which promotes fouling [111]. Here, since the modified TFC (TFC3) showed a lower RSF than the TFC0, it has a lower tendency to fouling, as confirmed by the experiments.

In the control membrane, the combined BSA and MPs caused a higher flux decline compared to BSA and MPs alone (Fig. 6A) which is related to the synergistic effect of foulants copresence in the FS [12,112–114]. When BSA and MPs were present in the FS, BSA could be adsorbed on the surface of MPs forming a MP-BSA complex due to the electrostatic forces [2] that is illustrated in Fig. 6B. The complex has a higher tendency to adhere to the membrane surface due to its hydrophobic nature [115]. Several studies have shown that the presence of multiple types of foulants in a feed solution can lead to a synergistic effect that causes a faster decline in membrane flux compared to individual foulants. For instance, Li and Elimelech [114] found that foulant accumulation on the NF membrane surface was faster in the presence of combined organic foulants and colloidal particles than when each foulant was present alone. Similarly, Li et al. [112] investigated the synergistic fouling effects of silica and humic acid (HA) in the reverse osmosis (RO) process and reported higher fouling effects of combined silica and HA. The copresence of protein and silica particles synergistically increased the flux decline of RO membranes in another study conducted by Quay et al. [113]. Similarly, the combined fouling impact of alginate and silica colloids was reported in FO membranes [116]. Hence, the presence of multiple types of foulants in FS can aggravate fouling causing a faster decline in membrane flux compared to individual foulants. However, when considering the modified membrane (TFC03), the difference between BSA alone and combined BSA and MPs was lower than their difference in TFC0. This can be attributed to higher hydrophilicity of modified membrane that reduces the adsorption of MPs and BSA and subsequently their complex leading to a lower flux decline.

In addition, flux recovery rates of both membranes after fouling experiments were measured to determine the irreversibility of the fouling. Both control and modified membranes showed high flux recovery after MP fouling, indicating the low irreversible fouling that is related to the low concentration of MPs (i.e., 10 ppm). TFC0 showed flux recoveries of 82% after BSA fouling and 73% after fouling of combined BSA and MPs while TFC3 showed almost full flux recoveries for both foulants. The modified membrane (TFC3) had a smoother and more hydrophilic surface that decreased the adhesion area for the foulants [44]. SEM images of the TFC0 and TFC3 after fouling experiments of combined BSA and MPs followed by physical cleaning are presented in Fig. 6C and D, respectively. As evident, a foulant layer of BSA and MPs covered the surface of TFC0 (Fig. 6C) (yellow arrows indicate foulants on the membrane surface) while this foulant layer was not found on the TFC3 (Fig. 6D). This is related to the fact that an increase in the hydrophilicity of the membrane surface significantly reduces the protein fouling owing to unfavorable polar interactions as protein molecules cannot displace the bound of the hydration layer to get adsorbed on the membrane [74]. That is in agreement with the flux recovery data. Overall, the modified TFC membrane demonstrated a lower fouling tendency and higher flux recovery than the control TFC membrane affirming the promise of integrating MIL-53(Fe) in TFC substrate layers for developing efficient TFC FO membranes for MPs treatment.

4. Conclusion

This research developed novel TFC FO membranes by incorporating various concentrations of as-synthesized MIL-53(Fe) into PSf substrates. The PSf characterizations showed higher hydrophilicity, roughness, and porosity of the modified substrates. The optimized TFC FO membrane (with 0.2 wt% MIL-53(Fe) loading rate in PSf substrate) indicated a smoother and more hydrophilic surface having a more nodular structure. The presence of MIL-53(Fe) increased the porosity and hydrophilicity of the substrates leading to a higher water flux (e.g., 11.4 LMH for the optimum modified FO membrane compared to 6 LMH for the control FO membrane). In addition, modified TFC FO membranes showed lower RSF (e.g., RSF of 5.08 g/m^{2}h for the optimum modified FO membrane compared to RSF of 6.30 g/m^{2}h for the control FO membrane). Moreover, the antifouling property of the control and optimum modified membranes against organic foulants (i.e., BSA), MPs, and combined BSA and MPs were investigated. The results indicated that the control and modified membranes had a flux decline of 60% and 29% for FS containing combined BSA and MPs, respectively. In addition, the control membrane had a flux recovery of 73%, while the modified membrane had a full flux recovery after the physical cleaning. The better antifouling characteristics can be attributed to the formation of a smoother and more hydrophilic PA layer on its surface, lower RSF, and lower ICP. The significant improvements in the performance and antifouling behavior of the developed membranes confirm that MIL-53(Fe) is a promising additive for modifying TFC FO membranes for high-performance membranes that are also robust against MPs and organic foulants.

Author contributions statement

Mitra Golgoli: Conceptualization, Investigation, Methodology, Formal analysis, Writing - original draft. Javad Farahbakhsh: Investigation, Methodology. Abdul Hannan Asif: Investigation, Methodology. Associate Professor Mehdi Khiadani: Conceptualization, Supervision, Writing - review & editing. Dr. Amir Razmjou: Writing - review & editing. Professor Michael Johns: Conceptualization, Supervision, Writing - review & editing. Dr. Masoumeh Zargar: Conceptualization, Supervision, Funding acquisition, Project administration, Writing - review & editing.

Declaration of competing interest

The authors declare that they have no known competing financial interests or personal relationships that could have appeared to influence the work reported in this paper.

Data availability

Data will be made available on request.

Acknowledgment

Funding from the Australian Research Council (ARC DECRA G1005399) for Dr. Masoumeh Zargar is gratefully acknowledged. The authors would also like to acknowledge the AMP Foundation for their generous support on the AMP Tomorrow Makers Award towards this project. The authors are also thankful to the Centre for Microscopy, Characterization & Analysis (CMCA), The University of Western Australia for facilities and Dr. Alexandra Suvorova for providing the technical support for microscopic analysis.

Appendix A. Supplementary data

Supplementary data to this article can be found online at https://doi.org/10.1016/j.memsci.2023.121766.

References

[1] Y. Xiang, L. Jiang, Y. Zhou, Z. Luo, D. Zhi, J. Yang, S.S. Lam, Microplastics and environmental pollutants: key interaction and toxicology in aquatic and soil environments, J. Hazard Mater. 422 (2022), 126843, https://doi.org/10.1016/J.JHAZMAT.2021.126843.

[2] P. Ju, Y. Zhang, Y. Zheng, F. Gao, F. Jiang, J. Li, C. Sun, Probing the toxic interactions between polyvinyl chloride microplastics and Human Serum Albumin by multispectroscopic techniques, Sci. Total Environ. 734 (2020), 139219, https://doi.org/10.1016/J.SCITOTENV.2020.139219.

[3] Z. Wang, M. Sedighi, A. Lea-Langton, Filtration of microplastic spheres by biochar: removal efficiency and immobilisation mechanisms, Water Res. 184 (2020), 116165, https://doi.org/10.1016/J.WATRES.2020.116165.

[4] J. Sun, X. Dai, Q. Wang, M.C.M. van Loosdrecht, B.-J. Ni, Microplastics in wastewater treatment plants: detection, occurrence and removal, Water Res. 152 (2019) 21–37, https://doi.org/10.1016/j.watres.2018.12.050.

[5] M. Golgoli, M. Khiadani, A. Shafieian, T.K. Sen, Y. Hartanto, M.L. Johns, M. Zargar, Microplastics fouling and interaction with polymeric membranes: a review, Chemosphere 283 (2021), 131185, https://doi.org/10.1016/J.CHEMOSPHERE.2021.131185.

[6] M. Golmohammadi, S. Fatemeh Musavi, M. Habibi, R. Maleki, M. Golgoli, M. Zargar, L.F. Dumée, S. Baroutian, A. Razmjou, Molecular mechanisms of microplastics degradation: a review, Sep. Purif. Technol. 309 (2023), 122906, https://doi.org/10.1016/J.SEPPUR.2022.122906.

[7] M. Simon, N. van Alst, J. Vollertsen, Quantification of microplastic mass and removal rates at wastewater treatment plants applying Focal Plane Array (FPA)-based Fourier Transform Infrared (FT-IR) imaging, Water Res. 142 (2018) 1–9, https://doi.org/10.1016/j.watres.2018.05.019.

[8] Y. Hartanto, M. Zargar, X. Cui, B. Jin, S. Dai, Non-ionic copolymer microgels as high-performance draw materials for forward osmosis desalination, J. Membr. Sci. 572 (2019) 480–488, https://doi.org/10.1016/J.MEMSCI.2018.11.042.

[9] S. Zou, M. Qin, Z. He, Tackle reverse solute flux in forward osmosis towards sustainable water recovery: reduction and perspectives, Water Res. 149 (2019) 362–374, https://doi.org/10.1016/J.WATRES.2018.11.015.

[10] R.R. Gonzales, L. Zhang, Y. Sasaki, W. Kushida, H. Matsuyama, H.K. Shon, Facile development of comprehensively fouling-resistant reduced polyketone-based thin film composite forward osmosis membrane for treatment of oily wastewater, J. Membr. Sci. 626 (2021), 119185, https://doi.org/10.1016/J.MEMSCI.2021.119185.

[11] R. Li, S. Braekevelt, J.L.N. De Carfort, S. Hussain, U.E. Bollmann, K. Bester, Laboratory and pilot evaluation of aquaporin-based forward osmosis membranes for rejection of micropollutants, Water Res. 194 (2021), 116924, https://doi.org/10.1016/J.WATRES.2021.116924.

[12] M. Golgoli, M. Khiadani, T.K. Sen, A. Razmjou, M.L. Johns, M. Zargar, Synergistic effects of microplastics and organic foulants on the performance of forward osmosis membranes, Chemosphere 311 (2023), 136906, https://doi.org/10.1016/J.CHEMOSPHERE.2022.136906.

[13] Y. Hartanto, M. Zargar, H. Wang, B. Jin, S. Dai, Thermoresponsive acidic microgels as functional draw agents for forward osmosis desalination, Environ. Sci. Technol. 50 (2016) 4221–4228, https://doi.org/10.1021/ACS.EST.5B04123/SUPPL_FILE/ES5B04123_SI_001.PDF.

[14] M. Zargar, R. Ujihara, S.J. Vogt, J.S. Vrouwenvelder, E.O. Fridjonsson, M. L. Johns, Imaging of membrane concentration polarization by NaCl using 23Na nuclear magnetic resonance, J. Membr. Sci. 600 (2020), 117868, https://doi.org/10.1016/J.MEMSCI.2020.117868.

[15] V. Sanahuja-Embuena, J. Frauholz, T. Oruc, K. Trzaskus, C. Hélix-Nielsen, Transport mechanisms behind enhanced solute rejection in forward osmosis compared to reverse osmosis mode, J. Membr. Sci. 636 (2021), 119561, https://doi.org/10.1016/J.MEMSCI.2021.119561.

[16] P.S. Goh, A.F. Ismail, B.C. Ng, M.S. Abdullah, Recent progresses of forward osmosis membranes formulation and design for wastewater treatment, Water 11 (2019) 2043, https://doi.org/10.3390/W11102043, 11 (2019) 2043.

[17] P. Deka, V.K. Verma, A. Chandrasekaran, A.B. Neog, A. Bardhan, K. Raidongia, S. Subbiah, Performance of novel sericin doped reduced graphene oxide membrane for FO based membrane crystallization application, J. Membr. Sci. 660 (2022), 120884, https://doi.org/10.1016/J.MEMSCI.2022.120884.

[18] W. Suwaileh, M. Zargar, A. Abdala, F.A. Siddiqui, M. Khiadani, A. Abdel-Wahab, Concentration polarization control in stand-alone and hybrid forward osmosis systems: recent technological advancements and future directions, Chem. Eng. Res. Des. 178 (2022) 199–223, https://doi.org/10.1016/J.CHERD.2021.12.031.

[19] M. Kahrizi, J. Lin, G. Ji, L. Kong, C. Song, L.F. Dumée, S. Sahebi, S. Zhao, Relating forward water and reverse salt fluxes to membrane porosity and tortuosity in forward osmosis: CFD modelling, Sep. Purif. Technol. 241 (2020), 116727, https://doi.org/10.1016/J.SEPPUR.2020.116727.

[20] S. Lee, C. Boo, M. Elimelech, S. Hong, Comparison of fouling behavior in forward osmosis (FO) and reverse osmosis (RO), J. Membr. Sci. 365 (2010) 34–39, https://doi.org/10.1016/J.MEMSCI.2010.08.036.

[21] J.S. Yong, W.A. Phillip, M. Elimelech, Coupled reverse draw solute permeation and water flux in forward osmosis with neutral draw solutes, J. Membr. Sci. (2012) 392–393, https://doi.org/10.1016/J.MEMSCI.2011.11.020, 9–17.

[22] C.Y. Tang, Q. She, W.C.L. Lay, R. Wang, A.G. Fane, Coupled effects of internal concentration polarization and fouling on flux behavior of forward osmosis membranes during humic acid filtration, J. Membr. Sci. 354 (2010) 123–133, https://doi.org/10.1016/J.MEMSCI.2010.02.059.

[23] M. Arjmandi, M. Peyravi, M. Pourafshari Chenar, M. Jahanshahi, A new concept of MOF-based PMM by modification of conventional dense film casting method: significant impact on the performance of FO process, J. Membr. Sci. 579 (2019) 253–265, https://doi.org/10.1016/J.MEMSCI.2019.02.020.

[24] E. Nagy, I. Hegedüs, E.W. Tow, J.H. Lienhard V, Effect of fouling on performance of pressure retarded osmosis (PRO) and forward osmosis (FO), J. Membr. Sci. 565 (2018) 450–462, https://doi.org/10.1016/J.MEMSCI.2018.08.039.

[25] Q.V. Ly, Y. Hu, J. Li, J. Cho, J. Hur, Characteristics and influencing factors of organic fouling in forward osmosis operation for wastewater applications: a comprehensive review, Environ. Int. 129 (2019) 164–184, https://doi.org/10.1016/J.ENVINT.2019.05.033.

[26] F.A. Siddiqui, Q. She, A.G. Fane, R.W. Field, Exploring the differences between forward osmosis and reverse osmosis fouling, J. Membr. Sci. 565 (2018) 241–253, https://doi.org/10.1016/J.MEMSCI.2018.08.034.

[27] Y. Kim, L.H. Kim, J.S. Vrouwenvelder, N. Ghaffour, Effect of organic micropollutants on biofouling in a forward osmosis process integrating seawater desalination and wastewater reclamation, J. Hazard Mater. 401 (2021), 123386, https://doi.org/10.1016/J.JHAZMAT.2020.123386.

[28] Q. She, R. Wang, A.G. Fane, C.Y. Tang, Membrane fouling in osmotically driven membrane processes: a review, J. Membr. Sci. 499 (2016) 201–233, https://doi.org/10.1016/J.MEMSCI.2015.10.040.

[29] W. Suwaileh, N. Pathak, H. Shon, N. Hilal, Forward osmosis membranes and processes: a comprehensive review of research trends and future outlook, Desalination 485 (2020), 114455, https://doi.org/10.1016/J.DESAL.2020.114455.

[30] S. Yadav, H. Saleem, I. Ibrar, O. Naji, A.A. Hawari, A.A. Alanezi, S.J. Zaidi, A. Altaee, J. Zhou, Recent developments in forward osmosis membranes using carbon-based nanomaterials, Desalination 482 (2020), 114375, https://doi.org/10.1016/J.DESAL.2020.114375.

[31] N.D. Suzaimi, P.S. Goh, A.F. Ismail, S.C. Mamah, N.A.N.N. Malek, J.W. Lim, K. C. Wong, N. Hilal, Strategies in forward osmosis membrane substrate fabrication and modification: a review, Membrane 10 (2020) 332, https://doi.org/10.3390/MEMBRANES10110332, 10 (2020) 332.

[32] W. Wu, Y. Shi, G. Liu, X. Fan, Y. Yu, Recent development of graphene oxide based forward osmosis membrane for water treatment: a critical review, Desalination 491 (2020), 114452, https://doi.org/10.1016/J.DESAL.2020.114452.

[33] W.J. Lee, P.S. Goh, W.J. Lau, C.S. Ong, A.F. Ismail, Antifouling zwitterion embedded forward osmosis thin film composite membrane for highly concentrated oily wastewater treatment, Sep. Purif. Technol. 214 (2019) 40–50, https://doi.org/10.1016/J.SEPPUR.2018.07.009.

[34] W.F. Chan, E. Marand, S.M. Martin, Novel zwitterion functionalized carbon nanotube nanocomposite membranes for improved RO performance and surface anti-biofouling resistance, J. Membr. Sci. 509 (2016) 125–137, https://doi.org/10.1016/J.MEMSCI.2016.02.014.

[35] L. Joseph, B.M. Jun, M. Jang, C.M. Park, J.C. Muñoz-Senmache, A.J. Hernández-Maldonado, A. Heyden, M. Yu, Y. Yoon, Removal of contaminants of emerging concern by metal-organic framework nanoadsorbents: a review, Chem. Eng. J. 369 (2019) 928–946, https://doi.org/10.1016/J.CEJ.2019.03.173.

[36] S. Samsami, M.H. Sarrafzadeh, A. Ahmadi, Surface modification of thin-film nanocomposite forward osmosis membrane with super-hydrophilic MIL-53 (Al) for doxycycline removal as an emerging contaminant and membrane antifouling property enhancement, Chem. Eng. J. 431 (2022), 133469, https://doi.org/10.1016/J.CEJ.2021.133469.

[37] D. Salionov, O.O. Semivrazhskaya, N.P.M. Casati, M. Ranocchiari, S. Bjelić, R. Verel, J.A. van Bokhoven, V.L. Sushkevich, Unraveling the molecular mechanism of MIL-53(Al) crystallization, Nat. Commun 131 (13) (2022) 1–9, https://doi.org/10.1038/s41467-022-31294-4, 2022.

[38] M. He, L. Wang, Y. Lv, X. Wang, J. Zhu, Y. Zhang, T. Liu, Novel polydopamine/metal organic framework thin film nanocomposite forward osmosis membrane for salt rejection and heavy metal removal, Chem. Eng. J. 389 (2020), 124452, https://doi.org/10.1016/j.cej.2020.124452.

[39] X. Wang, X. Ba, N. Cui, Z. Ma, L. Wang, Z. Wang, X. Gao, Preparation, characterisation, and desalination performance study of cellulose acetate membranes with MIL-53(Fe) additive, J. Membr. Sci. 590 (2019), 117057, https://doi.org/10.1016/J.MEMSCI.2019.04.061.
[40] M. Kadhom, B. Deng, Metal-organic frameworks (MOFs) in water filtration membranes for desalination and other applications, Appl. Mater. Today 11 (2018) 219–230, https://doi.org/10.1016/J.APMT.2018.02.008.
[41] W. Fu, J. Chen, C. Li, L. Jiang, M. Qiu, X. Li, Y. Wang, L. Cui, Enhanced flux and fouling resistance forward osmosis membrane based on a hydrogel/MOF hybrid selective layer, J. Colloid Interface Sci. 585 (2021) 158–166, https://doi.org/10.1016/J.JCIS.2020.11.092.
[42] M. Qiu, C. He, Efficient removal of heavy metal ions by forward osmosis membrane with a polydopamine modified zeolitic imidazolate framework incorporated selective layer, J. Hazard Mater. 367 (2019) 339–347, https://doi.org/10.1016/J.JHAZMAT.2018.12.096.
[43] M. Bagherzadeh, A. Bayrami, M. Amini, Enhancing forward osmosis (FO) performance of polyethersulfone/polyamide (PES/PA) thin-film composite membrane via the incorporation of GQDs@UiO-66-NH2 particles, J. Water Process Eng. 33 (2020), 101107, https://doi.org/10.1016/j.jwpe.2019.101107.
[44] A. Bayrami, M. Bagherzadeh, H. Navi, M. Chegeni, M. Hosseinifard, M. Amini, Thin-film nanocomposite membranes containing aspartic acid-modified MIL-53-NH2 (Al) for boosting desalination and anti-fouling performance, Desalination 521 (2022), 115386, https://doi.org/10.1016/J.DESAL.2021.115386.
[45] Y. Xu, X. Gao, Q. Wang, X. Wang, Z. Ji, C. Gao, Highly stable MIL-101(Cr) doped water permeable thin film nanocomposite membranes for water treatment, RSC Adv. 6 (2016) 82669–82675, https://doi.org/10.1039/C6RA16896E.
[46] D. Ma, S.B. Peh, G. Han, S.B. Chen, Thin-film nanocomposite (TFN) membranes incorporated with super-hydrophilic metal-organic framework (MOF) UiO-66: toward enhancement of water flux and salt rejection, ACS Appl. Mater. Interfaces 9 (2017) 7523–7534, https://doi.org/10.1021/ACSAMI.6B14223/ASSET/IMAGES/ACSAMI.6B14223.SOCIAL.JPEG_V03.
[47] T. Eghbalazar, A. Shakeri, High-Performance Thin-Film nanocomposite forward osmosis membranes modified with Poly(dopamine) coated UiO66-(COOH)2, Sep. Purif. Technol. 277 (2021), 119438, https://doi.org/10.1016/J.SEPPUR.2021.119438.
[48] D. Ma, G. Han, S.B. Peh, S.B. Chen, Water-stable metal-organic framework UiO-66 for performance enhancement of forward osmosis membranes, Ind. Eng. Chem. Res. 56 (2017) 12773–12782, https://doi.org/10.1021/ACS.IECR.7B03278/ASSET/IMAGES/LARGE/IE-2017-03278F_0008.JPEG.
[49] M. Arjmandi, M. Pourafshari Chenar, M. Peyravi, M. Jahanshahi, Physical modification of polymeric support layer for thin film composite forward osmosis membranes by metal–organic framework-based porous matrix membrane strategy, J. Appl. Polym. Sci. 137 (2020), 48672, https://doi.org/10.1002/APP.48672.
[50] M. Enfrin, J. Wang, A. Merenda, L.F. Dumée, J. Lee, Mitigation of membrane fouling by nano/microplastics via surface chemistry control, J. Membr. Sci. 633 (2021), 119379, https://doi.org/10.1016/J.MEMSCI.2021.119379.
[51] M. Enfrin, J. Lee, P. Le-Clech, L.F. Dumée, Kinetic and mechanistic aspects of ultrafiltration membrane fouling by nano- and microplastics, J. Membr. Sci. 601 (2020), 117890, https://doi.org/10.1016/J.MEMSCI.2020.117890.
[52] J. Li, B. Wang, Z. Chen, B. Ma, J.P. Chen, Ultrafiltration membrane fouling by microplastics with raw water: behaviors and alleviation methods, Chem. Eng. J. 410 (2021), 128174, https://doi.org/10.1016/j.cej.2020.128174.
[53] J.Y. Lee, Q. She, F. Huo, C.Y. Tang, Metal–organic framework-based porous matrix membranes for improving mass transfer in forward osmosis membranes, J. Membr. Sci. 492 (2015) 392–399, https://doi.org/10.1016/J.MEMSCI.2015.06.003.
[54] C.J. Wu, I. Valerie Maggay, C.H. Chiang, W. Chen, Y. Chang, C. Hu, A. Venault, Removal of tetracycline by a photocatalytic membrane reactor with MIL-53(Fe)/PVDF mixed-matrix membrane, Chem. Eng. J. 451 (2023), 138990, https://doi.org/10.1016/J.CEJ.2022.138990.
[55] J.O. Hsieh, K.J. Balkus, J.P. Ferraris, I.H. Musselman, MIL-53 frameworks in mixed-matrix membranes, Microporous Mesoporous Mater. 196 (2014) 165–174, https://doi.org/10.1016/J.MICROMESO.2014.05.006.
[56] X. Xiang, D. Chen, N. Li, Q. Xu, H. Li, J. He, J. Lu, Mil-53(Fe)-loaded polyacrylonitrile membrane with superamphiphilicity and double hydrophobicity for effective emulsion separation and photocatalytic dye degradation, Sep. Purif. Technol. 282 (2022), 119910, https://doi.org/10.1016/J.SEPPUR.2021.119910.
[57] M. Zargar, Y. Hartanto, B. Jin, S. Dai, Polyethylenimine modified silica nanoparticles enhance interfacial interactions and desalination performance of thin film nanocomposite membranes, J. Membr. Sci. 541 (2017) 19–28, https://doi.org/10.1016/J.MEMSCI.2017.06.085.
[58] M. Zargar, Y. Hartanto, B. Jin, S. Dai, Hollow mesoporous silica nanoparticles: a peculiar structure for thin film nanocomposite membranes, J. Membr. Sci. 519 (2016) 1–10, https://doi.org/10.1016/j.memsci.2016.07.052.
[59] M. Zargar, B. Jin, S. Dai, An integrated statistic and systematic approach to study correlation of synthesis condition and desalination performance of thin film composite membranes, Desalination 394 (2016) 138–147, https://doi.org/10.1016/j.desal.2016.05.014.
[60] M. Rastgar, A. Bozorg, A. Shakeri, Novel dimensionally controlled nanopore forming template in forward osmosis membranes, Environ. Sci. Technol. 52 (2018) 2704–2716, https://doi.org/10.1021/ACS.EST.7B05583/ASSET/IMAGES/LARGE/ES-2017-055835_0010.JPEG.
[61] A. Tiraferri, N.Y. Yip, A.P. Straub, S. Romero-Vargas Castrillon, M. Elimelech, A method for the simultaneous determination of transport and structural parameters of forward osmosis membranes, J. Membr. Sci. 444 (2013) 523–538, https://doi.org/10.1016/J.MEMSCI.2013.05.023.
[62] C. Lee, T.T. Nguyen, R.S. Adha, H.K. Shon, I.S. Kim, Influence of hydrodynamic operating conditions on organic fouling of spiral-wound forward osmosis membranes: fouling-induced performance deterioration in FO-RO hybrid system, Water Res. 185 (2020), 116154, https://doi.org/10.1016/J.WATRES.2020.116154.
[63] F. Ricceri, M. Giagnorio, K.R. Zodrow, A. Tiraferri, Organic fouling in forward osmosis: governing factors and a direct comparison with membrane filtration driven by hydraulic pressure, J. Membr. Sci. 619 (2021), 118759, https://doi.org/10.1016/J.MEMSCI.2020.118759.
[64] T.T. Nguyen, C. Lee, R.W. Field, I.S. Kim, Insight into organic fouling behavior in polyamide thin-film composite forward osmosis membrane: critical flux and its impact on the economics of water reclamation, J. Membr. Sci. 606 (2020), 118118, https://doi.org/10.1016/J.MEMSCI.2020.118118.
[65] H. Hidayaturrahman, T.-G. Lee, A study on characteristics of microplastic in wastewater of South Korea: identification, quantification, and fate of microplastics during treatment process, Mar. Pollut. Bull. 146 (2019) 696–702, https://doi.org/10.1016/j.marpolbul.2019.06.071.
[66] M. Shen, Y. Zhang, E. Almatrafi, T. Hu, C. Zhou, B. Song, Z. Zeng, G. Zeng, Efficient removal of microplastics from wastewater by an electrocoagulation process, Chem. Eng. J. 428 (2022), 131161, https://doi.org/10.1016/J.CEJ.2021.131161.
[67] T. Araya, M. Jia, J. Yang, P. Zhao, K. Cai, W. Ma, Y. Huang, Resin modified MIL-53 (Fe) MOF for improvement of photocatalytic performance, Appl. Catal. B Environ. 203 (2017) 768–777, https://doi.org/10.1016/J.APCATB.2016.10.072.
[68] M. Ionita, E. Vasile, L.E. Crica, S.I. Voicu, A.M. Pandele, S. Dinescu, L. Predoiu, B. Galateanu, A. Hermenean, M. Costache, Synthesis, characterization and in vitro studies of polysulfone/graphene oxide composite membranes, Compos. Part B Eng. 72 (2015) 108–115, https://doi.org/10.1016/J.COMPOSITESB.2014.11.040.
[69] Y. Ren, T. Li, W. Zhang, S. Wang, M. Shi, C. Shan, W. Zhang, X. Guan, L. Lv, M. Hua, B. Pan, MIL-PVDF blend ultrafiltration membranes with ultrahigh MOF loading for simultaneous adsorption and catalytic oxidation of methylene blue, J. Hazard Mater. 365 (2019) 312–321, https://doi.org/10.1016/J.JHAZMAT.2018.11.013.
[70] J. Ma, S. Li, G. Wu, S. Wang, X. Guo, L. Wang, X. Wang, J. Li, L. Chen, Preparation of mixed-matrix membranes from metal organic framework (MIL-53) and poly (vinylidene fluoride) for use in determination of sulfonylurea herbicides in aqueous environments by high performance liquid chromatography, J. Colloid Interface Sci. 553 (2019) 834–844, https://doi.org/10.1016/J.JCIS.2019.06.082.
[71] K. Vinothkumar, M. Shivanna Jyothi, C. Lavanya, M. Sakar, S. Valiyaveettil, R. G. Balakrishna, Strongly co-ordinated MOF-PSF matrix for selective adsorption, separation and photodegradation of dyes, Chem. Eng. J. 428 (2022), 132561, https://doi.org/10.1016/J.CEJ.2021.132561.
[72] M.S. Jyothi, S. Yadav, G. Balakrishna, Effective recovery of acids from egg waste incorporated PSf membranes: a step towards sustainable development, J. Membr. Sci. 549 (2018) 227–235, https://doi.org/10.1016/J.MEMSCI.2017.12.013.
[73] H. Karimi, M. Bazgar Bajestani, S.A. Mousavi, R. Mokhtari Garakani, Polyamide membrane surface and bulk modification using humid environment as a new heat curing medium, J. Membr. Sci. 523 (2017) 129–137, https://doi.org/10.1016/J.MEMSCI.2016.09.042.
[74] L. Huang, S. Zhao, Z. Wang, J. Wu, J. Wang, S. Wang, In situ immobilization of silver nanoparticles for improving permeability, antifouling and anti-bacterial properties of ultrafiltration membrane, J. Membr. Sci. 499 (2016) 269–281, https://doi.org/10.1016/J.MEMSCI.2015.10.055.
[75] Y. Chun, L. Qing, G. Sun, M.R. Bilad, A.G. Fane, T.H. Chong, Prototype aquaporin-based forward osmosis membrane: filtration properties and fouling resistance, Desalination 445 (2018) 75–84, https://doi.org/10.1016/J.DESAL.2018.07.030.
[76] J. Jung, J. Ryu, Y. Yu, J. Kweon, Characteristics of organic fouling, reversibility by physical cleaning and concentrates in forward osmosis membrane processes for wastewater reclamation, Chemosphere 245 (2020), 125787, https://doi.org/10.1016/J.CHEMOSPHERE.2019.125787.
[77] G. Ye, J. Lee, F. Perreault, M. Elimelech, Controlled architecture of dual-functional block copolymer brushes on thin-film composite membranes for integrated “defending” and “attacking” strategies against biofouling, ACS Appl. Mater. Interfaces 7 (2015) 23069–23079, https://doi.org/10.1021/ACSAMI.5B06647/ASSET/IMAGES/LARGE/AM-2015-06647P_0007.JPEG.
[78] S. Ahmadipouya, S.A. Mousavi, A. Shokrgozar, D.V. Mousavi, Improving dye removal and antifouling performance of polysulfone nanofiltration membranes by incorporation of UiO-66 metal-organic framework, J. Environ. Chem. Eng. 10 (2022), 107535, https://doi.org/10.1016/J.JECE.2022.107535.
[79] J. María Arsuaga, A. Sotto, G. del Rosario, A. Martínez, S. Molina, S.B. Teli, J. de Abajo, Influence of the type, size, and distribution of metal oxide particles on the properties of nanocomposite ultrafiltration membranes, J. Membr. Sci. 428 (2013) 131–141, https://doi.org/10.1016/J.MEMSCI.2012.11.008.
[80] H. Mahdavi, M. Karami, A.A. Heidari, P.K. kahriz, Preparation of mixed matrix membranes made up of polysulfone and MIL-53(Al) nanoparticles as promising membranes for separation of aqueous dye solutions, Sep. Purif. Technol. 274 (2021), 119033, https://doi.org/10.1016/J.SEPPUR.2021.119033.
[81] H.M. Park, K.Y. Jee, Y.T. Lee, Preparation and characterization of a thin-film composite reverse osmosis membrane using a polysulfone membrane including metal-organic frameworks, J. Membr. Sci. 541 (2017) 510–518, https://doi.org/10.1016/J.MEMSCI.2017.07.034.
[82] S. Morales-Torres, C.M.P. Esteves, J.L. Figueiredo, A.M.T. Silva, Thin-film composite forward osmosis membranes based on polysulfone supports blended

with nanostructured carbon materials, J. Membr. Sci. 520 (2016) 326–336, https://doi.org/10.1016/J.MEMSCI.2016.07.009.
[83] A. Xie, J. Cui, J. Yang, Y. Chen, J. Lang, C. Li, Y. Yan, J. Dai, Photo-Fenton self-cleaning PVDF/NH2-MIL-88B(Fe) membranes towards highly-efficient oil/water emulsion separation, J. Membr. Sci. 595 (2020), 117499, https://doi.org/10.1016/J.MEMSCI.2019.117499.
[84] X. Liu, H.Y. Ng, Fabrication of layered silica–polysulfone mixed matrix substrate membrane for enhancing performance of thin-film composite forward osmosis membrane, J. Membr. Sci. 481 (2015) 148–163, https://doi.org/10.1016/J.MEMSCI.2015.02.012.
[85] H. Salehi, A. Shakeri, H. Mahdavi, R.G.H. Lammertink, Improved performance of thin-film composite forward osmosis membrane with click modified polysulfone substrate, Desalination 496 (2020), 114731, https://doi.org/10.1016/J.DESAL.2020.114731.
[86] Y. Wang, T. Xu, Anchoring hydrophilic polymer in substrate: an easy approach for improving the performance of TFC FO membrane, J. Membr. Sci. 476 (2015) 330–339, https://doi.org/10.1016/J.MEMSCI.2014.11.025.
[87] A.P. Bendoy, H.G. Zeweldi, M.J. Park, H.K. Shon, H. Kim, W.J. Chung, G. M. Nisola, Silicene nanosheets as support fillers for thin film composite forward osmosis membranes, Desalination 536 (2022), 115817, https://doi.org/10.1016/J.DESAL.2022.115817.
[88] J. Ma, X. Guo, Y. Ying, D. Liu, C. Zhong, Composite ultrafiltration membrane tailored by MOF@GO with highly improved water purification performance, Chem. Eng. J. 313 (2017) 890–898, https://doi.org/10.1016/J.CEJ.2016.10.127.
[89] F. Huang, Q. Wang, Q. Wei, W.G. E P, U, Dynamic Wettability and Contact Angles of Poly (Vinylidene Fluoride) Nanofiber Membranes Grafted with Acrylic Acid, Expresspolymlett.Com, 2010, https://doi.org/10.3144/expresspolymlett.2010.69, 2010.
[90] R.S. Hebbar, A.M. Isloor, A.F. Ismail, Contact angle measurements, Membr. Charact. (2017) 219–255, https://doi.org/10.1016/B978-0-444-63776-5.00012-7.
[91] S. Shokrgozar Eslah, S. Shokrollahzadeh, O. Moini Jazani, A. Samimi, Forward Osmosis Water Desalination: Fabrication of Graphene Oxide-Polyamide/polysulfone Thin-Film Nanocomposite Membrane with High Water Flux and Low Reverse Salt Diffusion, 2017, pp. 573–583, https://doi.org/10.1080/01496395.2017.1398261, 10.1080/01496395.2017.1398261. 53.
[92] M. Fathizadeh, A. Aroujalian, A. Raisi, Effect of lag time in interfacial polymerization on polyamide composite membrane with different hydrophilic sub layers, Desalination 284 (2012) 32–41, https://doi.org/10.1016/J.DESAL.2011.08.034.
[93] X. Lu, L.H. Arias Chavez, S. Romero-Vargas Castrillón, J. Ma, M. Elimelech, Influence of active layer and support layer surface structures on organic fouling propensity of thin-film composite forward osmosis membranes, Environ. Sci. Technol. 49 (2015) 1436–1444, https://doi.org/10.1021/ES5044062/SUPPL_FILE/ES5044062_SI_001.PDF.
[94] A.K. Ghosh, E.M.V. Hoek, Impacts of support membrane structure and chemistry on polyamide–polysulfone interfacial composite membranes, J. Membr. Sci. 336 (2009) 140–148, https://doi.org/10.1016/J.MEMSCI.2009.03.024.
[95] Z. Yang, Z.W. Zhou, H. Guo, Z. Yao, X.H. Ma, X. Song, S.P. Feng, C.Y. Tang, Tannic acid/Fe3+ nanoscaffold for interfacial polymerization: toward enhanced nanofiltration performance, Environ. Sci. Technol. 52 (2018) 9341–9349, https://doi.org/10.1021/ACS.EST.8B02425/ASSET/IMAGES/MEDIUM/ES-2018-02425Y_M003.GIF.
[96] M.T.M. Pendergast, A.K. Ghosh, E.M.V. Hoek, Separation performance and interfacial properties of nanocomposite reverse osmosis membranes, Desalination 308 (2013) 180–185, https://doi.org/10.1016/J.DESAL.2011.05.005.
[97] E. Bormashenko, Why does the Cassie–Baxter equation apply? Colloids Surfaces A Physicochem. Eng. Asp. 324 (2008) 47–50, https://doi.org/10.1016/J.COLSURFA.2008.03.025.
[98] J. Wang, Y. Wu, Y. Cao, G. Li, Y. Liao, Influence of surface roughness on contact angle hysteresis and spreading work, Colloid Polym. Sci. 298 (2020) 1107–1112, https://doi.org/10.1007/S00396-020-04680-X/FIGURES/4.
[99] H.N. Drikvand, M. Golgoli, M. Zargar, M. Ulbricht, S. Nejati, Y. Mansourpanah, Thermo-responsive hydrophilic support for polyamide thin-film composite membranes with competitive nanofiltration performance, Polym 14 (2022) 3376, https://doi.org/10.3390/POLYM14163376, 14 (2022) 3376.
[100] J.R. McCutcheon, M. Elimelech, Influence of membrane support layer hydrophobicity on water flux in osmotically driven membrane processes, J. Membr. Sci. 318 (2008) 458–466, https://doi.org/10.1016/j.memsci.2008.03.021.
[101] Q. Liu, J. Li, Z. Zhou, J. Xie, J.Y. Lee, Hydrophilic mineral coating of membrane substrate for reducing internal concentration polarization (ICP) in forward osmosis, Sci. Rep. 61 (6) (2016) 1–10, https://doi.org/10.1038/srep19593, 2016.
[102] N.N. Bui, J.R. McCutcheon, Hydrophilic nanofibers as new supports for thin film composite membranes for engineered osmosis, Environ. Sci. Technol. 47 (2013) 1761–1769, https://doi.org/10.1021/ES304215G/ASSET/IMAGES/LARGE/ES-2012-04215G_0005.JPEG.
[103] D. Emadzadeh, W.J. Lau, T. Matsuura, M. Rahbari-Sisakht, A.F. Ismail, A novel thin film composite forward osmosis membrane prepared from PSf–TiO2 nanocomposite substrate for water desalination, Chem. Eng. J. 237 (2014) 70–80, https://doi.org/10.1016/J.CEJ.2013.09.081.
[104] M. Ghanbari, D. Emadzadeh, W.J. Lau, H. Riazi, D. Almasi, A.F. Ismail, Minimizing structural parameter of thin film composite forward osmosis membranes using polysulfone/halloysite nanotubes as membrane substrates, Desalination 377 (2016) 152–162, https://doi.org/10.1016/J.DESAL.2015.09.019.
[105] X. Wu, R.W. Field, J.J. Wu, K. Zhang, Polyvinylpyrrolidone modified graphene oxide as a modifier for thin film composite forward osmosis membranes, J. Membr. Sci. 540 (2017) 251–260, https://doi.org/10.1016/J.MEMSCI.2017.06.070.
[106] S. Zhang, F. Fu, T.S. Chung, Substrate modifications and alcohol treatment on thin film composite membranes for osmotic power, Chem. Eng. Sci. 87 (2013) 40–50, https://doi.org/10.1016/J.CES.2012.09.014.
[107] J. She, H. Gao, Z. Song, L. Shi, S. Liu, J. Li, X. Lu, C. Wu, N-methylglucamine modified poly (vinyl chloride) support assists the construction of uniform dually charged nanofiltration membrane via interfacial polymerization, Sep. Purif. Technol. 307 (2023), 122674, https://doi.org/10.1016/J.SEPPUR.2022.122674.
[108] Y. Wang, Z. Fang, S. Zhao, D. Ng, J. Zhang, Z. Xie, Dopamine incorporating forward osmosis membranes with enhanced selectivity and antifouling properties, RSC Adv. 8 (2018) 22469–22481, https://doi.org/10.1039/C8RA03166E.
[109] A. Shakeri, H. Salehi, F. Ghorbani, M. Amini, H. Naslhajian, Polyoxometalate based thin film nanocomposite forward osmosis membrane: superhydrophilic, anti-fouling, and high water permeable, J. Colloid Interface Sci. 536 (2019) 328–338, https://doi.org/10.1016/J.JCIS.2018.10.069.
[110] T. Hwang, J.S. Oh, W. Yim, J. Do Nam, C. Bae, H.I. Kim, K.J. Kim, Ultrafiltration using graphene oxide surface-embedded polysulfone membranes, Sep. Purif. Technol. 166 (2016) 41–47, https://doi.org/10.1016/J.SEPPUR.2016.04.018.
[111] W.A. Suwaileh, D.J. Johnson, S. Sarp, N. Hilal, Advances in forward osmosis membranes: altering the sub-layer structure via recent fabrication and chemical modification approaches, Desalination 436 (2018) 176–201, https://doi.org/10.1016/J.DESAL.2018.01.035.
[112] D. Li, W. Lin, R. Shao, Y.X. Shen, X. Zhu, X. Huang, Interaction between humic acid and silica in reverse osmosis membrane fouling process: a spectroscopic and molecular dynamics insight, Water Res. 206 (2021), 117773, https://doi.org/10.1016/J.WATRES.2021.117773.
[113] A.N. Quay, T. Tong, S.M. Hashmi, Y. Zhou, S. Zhao, M. Elimelech, Combined organic fouling and inorganic scaling in reverse osmosis: role of protein-silica interactions, Environ. Sci. Technol. 52 (2018) 9145–9153, https://doi.org/10.1021/ACS.EST.8B02194/SUPPL_FILE/ES8B02194_SI_001.PDF.
[114] Q. Li, M. Elimelech, Synergistic effects in combined fouling of a loose nanofiltration membrane by colloidal materials and natural organic matter, J. Membr. Sci. 278 (2006) 72–82, https://doi.org/10.1016/J.MEMSCI.2005.10.045.
[115] C. Ma, Q. Li, J. Liu, H. Bao, L. Wang, B. Zhao, Z. Zhang, Forward osmosis treatment of algal-rich water: characteristics and mechanism of membrane fouling, J. Hazard Mater. 423 (2022), 126984, https://doi.org/10.1016/J.JHAZMAT.2021.126984.
[116] Y. Kim, M. Elimelech, H.K. Shon, S. Hong, Combined organic and colloidal fouling in forward osmosis: fouling reversibility and the role of applied pressure, J. Membr. Sci. 460 (2014) 206–212, https://doi.org/10.1016/J.MEMSCI.2014.02.038.
[118] S. Ghasemi, B. Yan, M. Zargar, N.N. Ling, E.O. Fridjonsson, M.L. Johns, Impact of Microplastics on Organic Fouling of Hollow Fiber Membranes, Chem. Eng. J. (2023), 143320. https://doi.org/10.1016/j.cej.2023.143320.